Continuously Beam-Steered Phased Array Antenna Using GaN Varactors for Millimeter-Wave Applications

Abdelaziz Hamdoun, F Medjdoub, Mohamed Himdi, Malek Zegaoui, Olivier Lafond

electronics

MDPI

Article

Continuously Beam-Steered Phased Array Antenna Using GaN Varactors for Millimeter-Wave Applications

Abdelaziz Hamdoun [1,*], Farid Medjdoub [2], Mohamed Himdi [3], Malek Zegaoui [2] and Olivier Lafond [3]

[1] Université de Poitiers, CNRS, XLIM, 86000 Poitiers, France
[2] French National Centre for Scientific Research (CNRS), Institute of Electronics, Microelectronics and Nanotechnology (IEMN), Av. Poincare, 59650 Villeneuve d'Ascq, France
[3] Institut d'Electronique et des Technologies du numeRique (IETR), Université de Rennes, 35000 Rennes, France
* Correspondence: abdelaziz.hamdoun@univ-poitiers.fr

Abstract: A continuously steerable beam patch antenna array employing a classical phase shifter based on GaN HEMTs is presented. Here, the GaN HEMTs are used as varactor diodes to achieve the tunability purpose. By controlling the DC bias of these varactors from −2 V to 2 V, the proposed array antenna can provide continuous beam steering from 0° to +25° in the azimuth plane at 41.20 GHz, while achieving a low side-lobe level and good impedance matching performances. Using GaN HEMTs as varactors to achieve beam steering capability has never been tried before to the best of our knowledge. The measurement results agree well with the simulation results and validate the effectiveness of the proposed beam steering based on GaN technology. This proposed phased array antenna will find numerous applications within future wireless communications systems, especially for millimeter-wave applications.

Keywords: phase shifter; antenna array; GaN HEMTs; mm wave applications

Citation: Hamdoun, A.; Medjdoub, F.; Himdi, M.; Zegaoui, M.; Lafond, O. Continuously Beam-Steered Phased Array Antenna Using GaN Varactors for Millimeter-Wave Applications. *Electronics* **2024**, *13*, 4698. https://doi.org/10.3390/electronics13234698

Academic Editor: Djuradj Budimir

Received: 9 October 2024
Revised: 6 November 2024
Accepted: 18 November 2024
Published: 28 November 2024

1. Introduction

Following on from the development of communication technology, modern wireless communication systems are moving more and more toward systems that are multitasking, miniaturized, less expensive, and robust. To this end, there is considerable interest in reconfigurable active integrated antennas (AIAs) with multiple capabilities and functions without enlarging their occupied volume [1,2].

Emerging wireless millimeter-wave applications such as 5G wireless communications, Internet-of-Things (IoT), automotive radar, and satellite communications have attracted huge interest in the research of AIA designs operating at multi-frequencies, employing beam steering, and handling significant power levels, which has been a great challenge for millimeter-wave systems [3,4]. Millimeter-wave bands are characterized by a high available bandwidth, offering the possibility of high-capacity wireless transmission at gigabit-per-second (Gbps) data rates. Despite this great bandwidth potentially available, the transmission of the signals with minimum losses and interference is going to be one of the most important factors of wireless millimeter-wave applications [5,6]. For this, some techniques such as beamforming will be used to improve the transmission of data; however, performing it at millimeter-wave frequencies will be a big challenge [6,7].

In addition, beam scanning has emerged as one of the major functions in active integrated antenna designs for wireless millimeter-wave applications [1,6]. Generally, antennas take the form of phased arrays, enabling beam scanning to be achieved by applying phase-shifted RF signals to each array element [8]. This kind of antenna design has the capability to steer the beam toward a specific direction while suppressing the unwanted beam in other directions, thus possessing many advantages such as saving sufficient energy, avoiding noisy environments, and overcoming the problems of radiation interference [6,9]. To achieve beam steering capability, analog phase shifters are therefore

crucial as RF components in phased array antenna systems, providing the suitable phase of each antenna element which can be adjusted for adaptive beam direction control. Various types of analog architectures have been proposed in the literature for phase control of the signals applied to the radiating elements making up an antenna array; they can be divided into two categories, analog active phase shifters and analog passives phase shifters [10–13].

One of the most useful topologies for analog phase shifters is the reflective structure employing a quadrature 3-dB 90° hybrid coupler using either lumped or distributed elements with two reflective loads at terminations [5,10]. Despite the advantages offered by this type of phase shifter in terms of design simplicity, linearity, and power consumption, two of its major drawbacks are that the overall insertion loss is usually high and also that the amplitude varies as a function of the synthesized phase shift [10,12]. Both of them can be important parameters that can limit the use of this topology. These insertion losses are directly related to the equivalent series resistor presented by the used varactor devices. On the other hand, a continuous phase shift can be easily accomplished when using a reflective structure for designing a phase shifter, thus allowing it to provide any desired phase shift.

Active devices such as varactor diodes are playing an important part in the design, development, and overall performance of wireless communication systems that require beam steering functionality; however, these devices present some non-linear behaviors, especially at high RF power levels, that impact the performances of antennas [14].

The superior characteristics of GaN technology, such as high-temperature operation due to large energy band gaps, high breakdown field, and high saturation velocities of electrons, make this semiconductor technology a promising candidate for achieving good linearity and realizing high-power and high-frequency varactor diodes; consequently, the designs of AIAs with high power handling capability and high-frequency operation are now easily achieved [15]. As a result, GaN-based HEMT semiconductor devices are no longer limited to high-power amplifier circuits [15], having now been extended to AIA systems [16,17]. Reconfigurable RF circuits, with high power/frequency and excellent linearity, are currently in great demand. GaN varactor diodes are among the key components in the design of these reconfigurable RF circuits to achieve the required performances for millimeter-wave applications. Furthermore, phased array antennas with beam steering capability at high power/frequency and with excellent efficiency have attracted a lot of research interest over the last few years.

Many research works using varactor diodes to obtain the beam steering functionality have already been reported in the literature. Most of them use GaAs varactors and thus result in a limitation in terms of frequency and RF power. This paper addresses the subject of a beam-steering phased array antenna based on a classical structure that is very known in the literature and which plays a vital part in wireless millimeter-wave applications. The array antenna is designed to continuously steer the main beam in continuous resolution without increasing the antenna elements or switching elements. The design of this antenna array has focused on developing the controllable continuous reflection type of phase shifter by using for the first time GaN HEMT varactor diodes as loads. Thus, this results in a novel beam-steering two-element patch antenna array using GaN HEMT components. The proposed overall objective of this research work is to demonstrate the realization of a large-signal continuous beam-scanning antenna array for millimeter-wave applications based on GaN technology which will be used as an active varactor co-integrated in low-cost microstrip technology to achieve the tunability of beams. The proposed phased antenna array design is based on existing designs of beam steering; here, GaN HEMT varactors are used for the first time for beam steering applications around 40 GHz.

This work can be divided into three major parts: the modeling of the GaN-based varactors, the phase shifter where these developed GaN devices are integrated, and the two-element patch array antenna. The completed study, simulation, and measurement of the GaN HEMTs as varactor devices are presented as well as the design of the used analog phase shifter and the two-element phased antenna array.

To the best of the authors' knowledge, this is the first time that GaN HEMTs have been used for an array antenna to achieve continuous beam steering.

2. Investigation of IEMN'S GaN Devices as Varactors

The realized active device, GaN_Lg110nm, studied here is based on the GaN process offered by the IEMN laboratory in Lille, France. The offered version of the IEMN-GaN HEMT structure that is used in this study features a gate length of 110 nm. This process is suitable for a 50 V drain voltage for power amplifier applications and yields current levels of ~1.3 A/mm. Figure 1a illustrates a photograph of the fabricated and analyzed device, while Figure 1b shows a simplified cross-section of the epitaxial layers of the GaN HEMT process developed by IEMN. More information about IEMN's GaN process features and limitations can be found in [18,19].

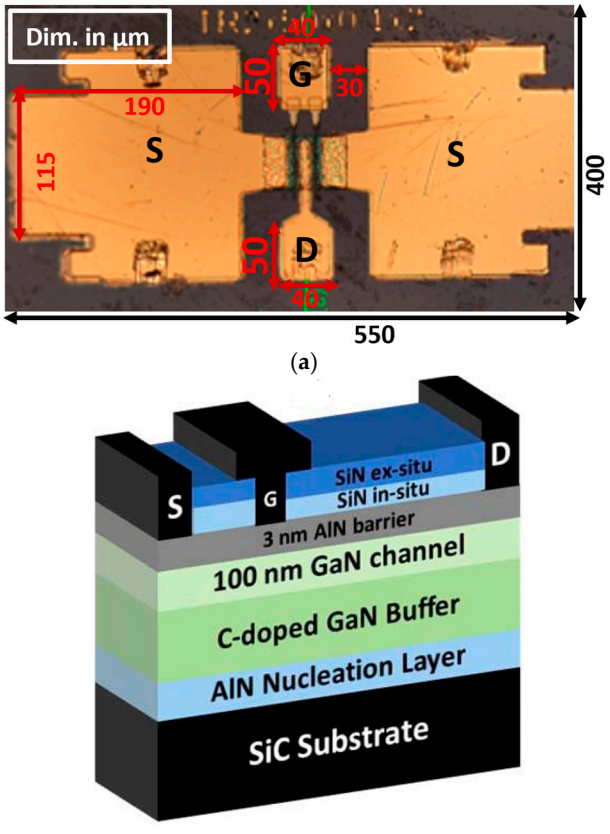

Figure 1. (**a**) Photograph of fabricated device "GaN_Lg110nm" and (**b**) schematic cross-section of IEMN's AlN/GaN-on-SiC HEMTs devices, showing contacts and epitaxial layers [18].

Many devices with different gate widths and lengths are available in the mask set and have been characterized in small and large signals [18]. However, only one sample called GaN_Lg110nm, with a gate length of 0.11 µm, a width of 50 µm, and a number of fingers of 2, is studied and used for the proposed phased antenna array. This device is selected for the design as it provides a tunable capacitance range from 32 fF to 355 fF at 40 GHz, which is the highest range compared to the other studied devices.

Temperature analysis has been performed on this device, and more details can be found in [19]. It is shown that over the 4 K to 400 K range, there is variation in the Hall electron mobility, sheet carrier density, and sheet resistance of the used HEMT structure. At liquid helium temperature (4 K), a state-of-the-art 2DEG mobility of 7340 $cm^2 \cdot V^{-1} \cdot s^{-1}$ combined with a sheet carrier density of 1.93 × 1013 cm^{-2} was measured, resulting in a remarkably low sheet resistance of 44 $\Omega/\square$.

Based on our previous works [15,20] on GaN varactor diode modeling of small and large signals, here, the same proposed equivalent circuit is used as a model to analyze the behavior of IEMN's GaN HEMT devices as varactors. The on-wafer RF measurements were performed by using IEMN's facilities over a frequency range of 0.25–67 GHz with a small RF power and a V_d fixed to 0 V, while V_g was varied from −7 V to +2 V. This allows us to realize a virtual connection from drain to source, resulting in a single Schottky junction which can be considered a planar Schottky varactor diode (PSVD) [15].

From the measurement, the extracted equivalent capacitance values, C_{Eq}, versus frequency are shown in Figure 2a. For V_g ranging from −7 V to −2 V, it is seen that the C_{Eq} values remain almost constant over all frequencies up to 20 GHz. Meanwhile, for V_g ranging from −1 V to +2 V, from 20 GHz, the C_{Eq} values start to increase exponentially due to high-frequency parasitic elements that become self-resonant at this bias voltage. More information about the extraction method can be found in [15,20].

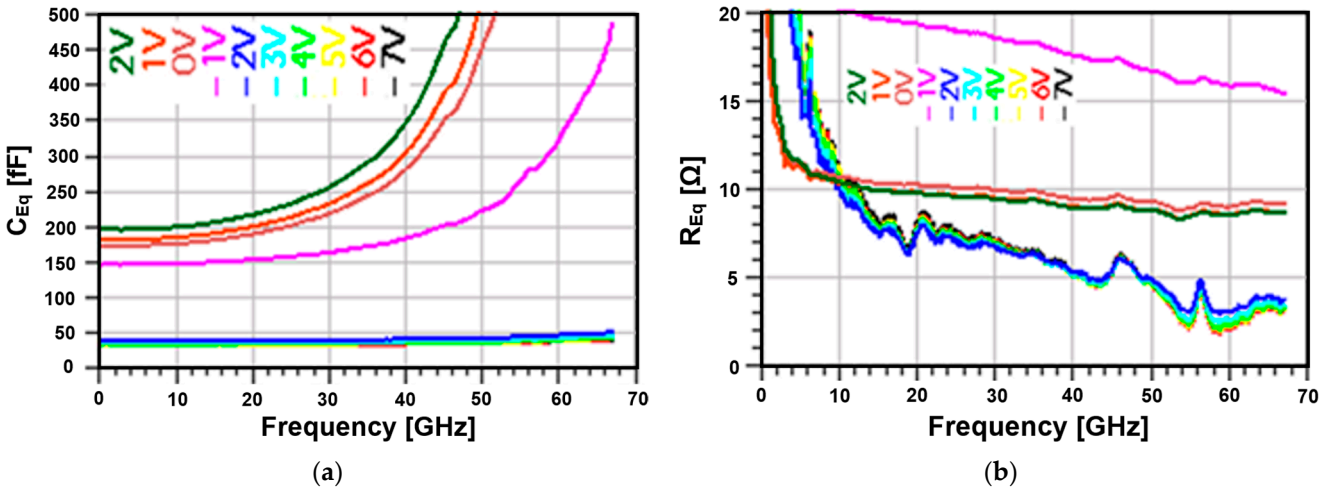

(**a**) (**b**)

Figure 2. (**a**) Extracted C_{Eq} and (**b**) extracted R_{Eq} vs. frequency for GaN_Lg110nm device.

Figure 2b illustrates the behavior of the extracted equivalent series resistance, R_{Eq}, versus frequency for various bias voltages V_g. Three ranges can be observed: in range_1, from −7 V to −2 V, the R_{Eq} values are at their minimum and decrease versus frequency. In range_2, from 0 V to +2 V, the R_{Eq} values increase compared to in range_1 and remain almost stable versus frequency. For V_g of −1 V, in range_3, the device exhibits its higher value of $R_{Eq,}$ which drops slightly with frequency. Because our frequency of interest is 40 GHz, here, the analysis of C_{Eq} and R_{Eq} is performed only at 40 GHz. The extracted tuning characteristic of C_{Eq} and R_{Eq} is plotted in Figure 3a,b.

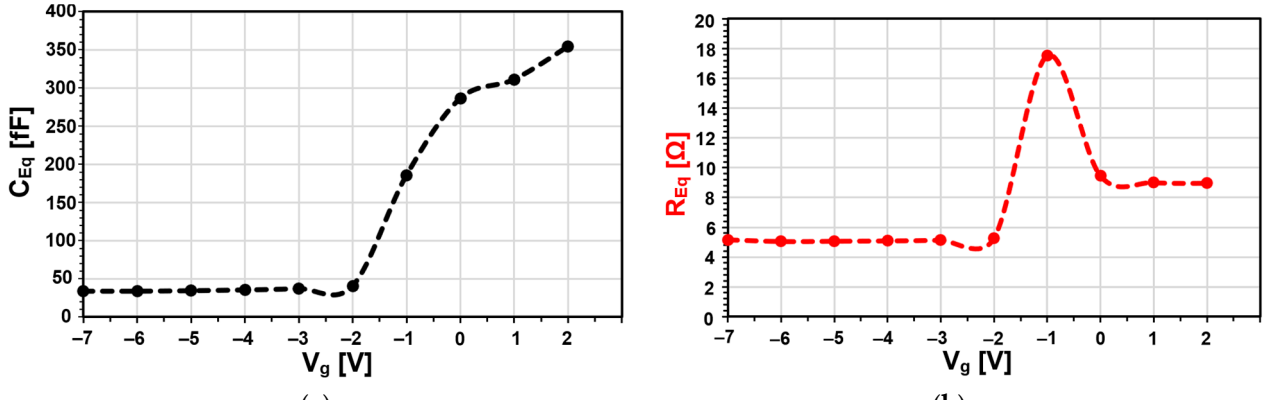

(**a**) (**b**)

Figure 3. (**a**) Extracted C_{Eq} and (**b**) R_{Eq} vs. V_g at 40 GHz for GaN_Lg110nm device.

The behavior of C_{Eq} vs. V_g can be separated into two regions:

- Region_1 for $-2\ V \leq V_g \leq 2\ V$: the C_{Eq} value changes significantly as does $R_{Eq,}$ where it achieves its maximum value of 18 Ω.
- Region_2 for $V_g < -2\ V$: Corresponding to C_{Eqmin}, the C_{Eq} value does not change. The same behavior is noticed for R_{Eq}.

As clearly seen, depending on the V_g value applied, tuning of the capacitive effect is generally achieved as a function of this bias voltage. In addition, as was already demonstrated in [15,20], a resistive effect can also be observed and it is also dependent on V_g. These two effects represent, respectively, the equivalent series capacitance (C_{Eq}) and the equivalent series resistance (R_{Eq}). As a result, this R_{Eq} will directly introduce more loss.

At 40 GHz, as seen in Figure 3a, the max and the min values of C_{Eq} are, respectively, 355 fF and 35 fF (C_{Eqmax}/C_{Eqmin} ratio about 10.4), achieved for the GaN_Lg110nm device.

3. Design of Analog GaN-Based Phase Shifter

This section discusses the design analysis of a mm-band phase shifter using GaN HEMT devices and based on the reflective structure employing a quadrature 3-dB 90° hybrid coupler, as illustrated in Figure 4a. The varactor, GaN_Lg110nm, at the "thru" and "coupled" ports reflects the signal with a tunable phase shift corresponding to its reactance, which is controlled by the gate bias voltage.

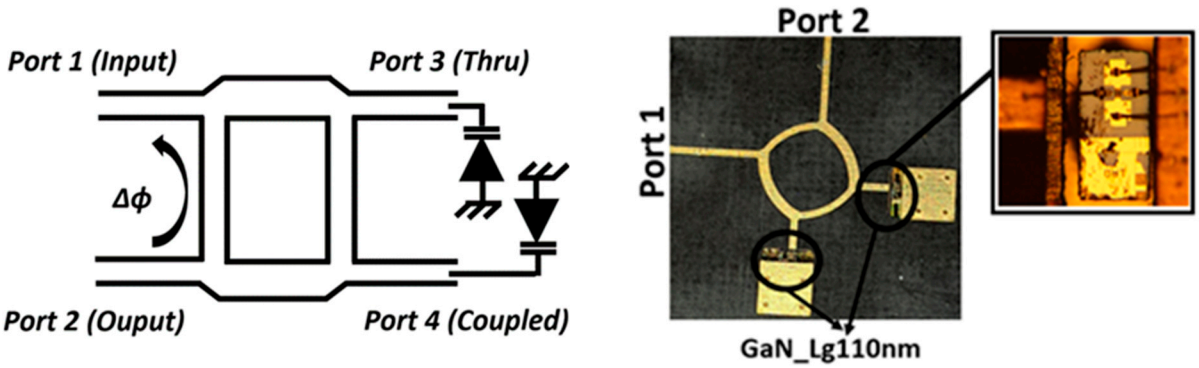

Figure 4. (**a**) A schematic illustration of the fabricated phase shifter, (**b**) a photograph of the fabricated phase shifter, (**c**) a zoomed-in image of one of the GaN_Lg110 devices along with the wire bonding.

Based on this phase shifter structure, one varactor diode placed at the two coupler output ports could be enough to achieve a theoretical phase shift of 180°, as explained in [21,22]. However, varactor diodes are not perfect. This means that there are losses due to their equivalent series resistance; also, these diodes have a limited tuning capacitance range, thus making it hard to achieve a 180° complete phase shift. This clearly limits the achievable beam steering range, which can be theoretically increased as much as wanted by multiplying the number of the used GaN varactors by a multiple of 2. However, more varactor diodes added will directly introduce more losses. This means that a tradeoff between beam steering range and losses should be defined, along with the targeted application where the phase shifter will be used.

The proposed phase shifter was designed using a low-permittivity substrate, Rogers RT5880 [23], with an ε_r of 2.2 and a thickness of 127 µm, and simulated using Advanced Design System (ADS) Momentum [24] proposed by Keysight. Here, the already developed GaN HEMT varactor small-signal model in [15] was used for the GaN_Lg110nm device as the tuning load. Two identical GaN_Lg110nm varactors were placed at the transmitted and coupled ports of the hybrid coupler. These two signals reflect from the two tunable loads, the GaN varactors; they add up in the phase at the hybrid's isolated port if both of the loads are identical and will keep matched the phase shifter's input signal.

Figure 4b depicts a photograph of the fabricated phase shifter. Wafer vias are used to connect the GaN varactors to the backside ground circuit metal. The wire bonding technique is used for all GaN varactors' PADs and was carried out at IETR's facilities. The overall size of this phase shifter design is 13×13 mm^2 and it was simulated and optimized to provide a maximum continuous phase shift at 41 GHz.

First, to design this phase shifter topology, a 3-dB 90° hybrid coupler has been designed and simulated. The Momentum-simulated layout results for the complete hybrid coupler are plotted in Figure 5. The insertion loss at port 3 and port 4 are, respectively, −0.40 dB and −0.25 dB at 41 GHz and has a maximum variation of −0.4 dB over a 2 GHz bandwidth from 40.50 GHz to 42.50 GHz. The amplitude imbalance at the center frequency is almost 0.15 dB. The phase difference between the outputs of ports 3 and 4 is about 87° at 41 GHz, while the return loss is greater than −20 dB and the isolation between the ports is greater than −25 dB. Now, the two output terminals will be loaded with the developed GaN_Lg110nm varactor small-signal model to achieve the phase shift purpose.

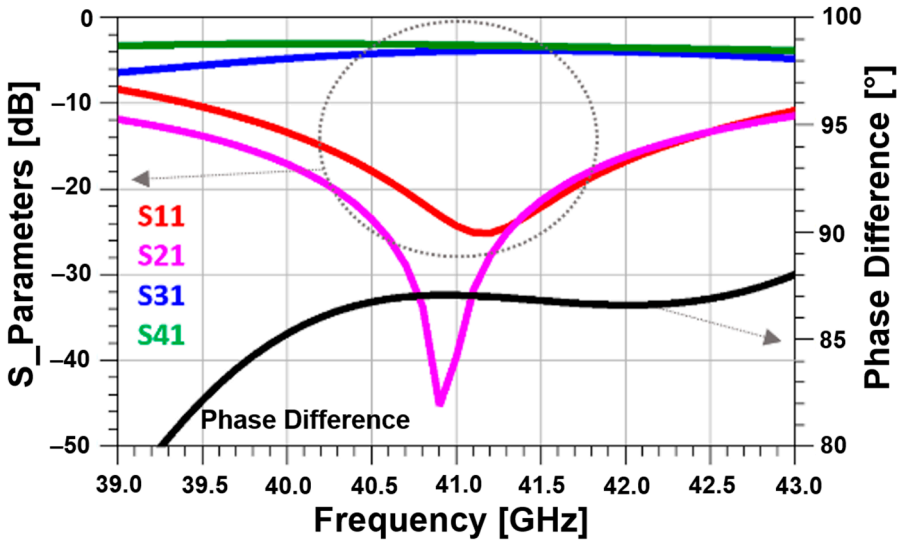

Figure 5. Simulated performances of hybrid coupler versus frequency.

Then, two identical GaN varactors, GaN_Lg110nm, were properly placed at the transmitted and coupled ports as tuning loads to provide the continuous tunability. Therefore, to discuss clearly the EM simulation as well as the measurement results, only two output phase shift difference values will be addressed and analyzed. Here, the two extreme values are chosen to conduct this analysis. Those values are achieved at a V_g of −2 V for the minimum value of the phase shift and at 2 V for the maximum value of the phase shift.

The phase shift versus frequency is plotted at −2 V and 2 V to compare the measured and simulated results in Figure 6. The simulation results show a continuously variable phase shift of up to 108°, while the measurements resulted in 110° tunability from 40 GHz to 42 GHz. As was almost expected, a good match between simulation and measurement is achieved at 40.5 GHz. However, it is shown that as the frequency becomes higher, more deviation is significant, while the phase difference between the maximum and the minimum values remains almost unchanged. This deviation can be caused by parasitic elements that are not captured in the proposed model.

In Figure 7, the return loss of the phase shifter under the two bias conditions is presented and is greater than −15 dB at 41 GHz. As can be clearly seen, a good match is achievable over the range of 40–42 GHz in simulations as well as in measurements.

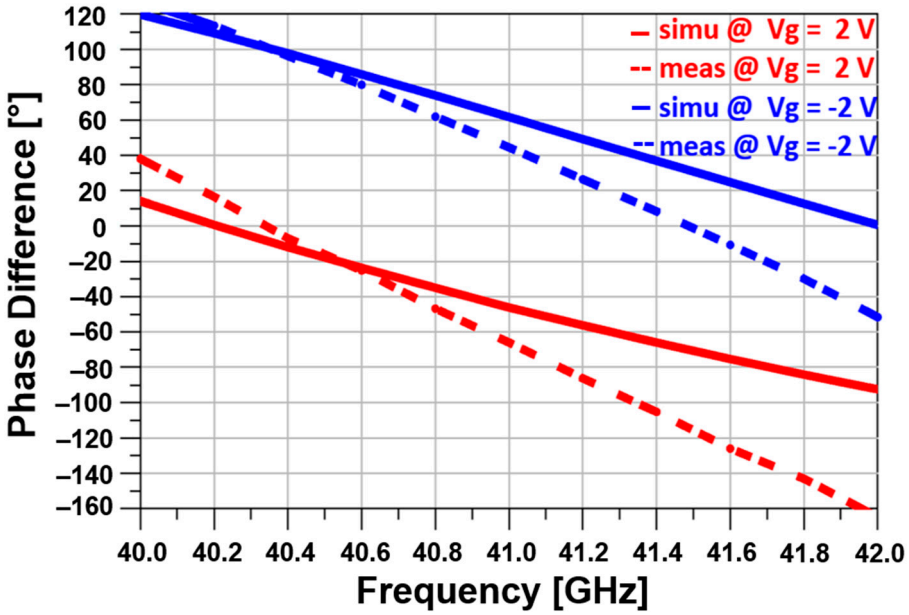

Figure 6. Simulated (continuous line) and measured (dotted line) phase states vs. frequency.

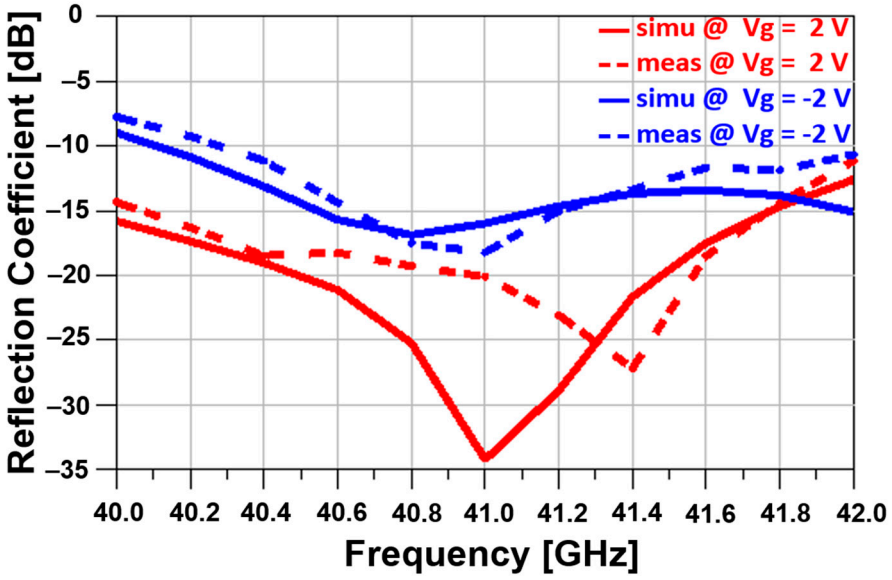

Figure 7. Simulated (continuous line) and measured (dotted line) |S11| versus frequency.

Figure 8 shows the simulated and measured insertion loss of the phase shifter at the two DC control voltages. The worst case of the insertion loss is about −4.5 dB and occurs at 40 GHz in the measurements. This value could be due to the higher series resistor value of the used HEMT device at this bias voltage [15,20] and also due to the wire bonding technique that is not included in the used HEMT varactor model. The amplitude imbalance between those two extreme DC bias states (i.e., −2 V and 2 V) is about 1.9 dB at 41.6 GHz and 2.7 dB at 40.6 GHz in simulations and in measurements and is therefore better than those values over the extended band from 40 to 42 GHz.

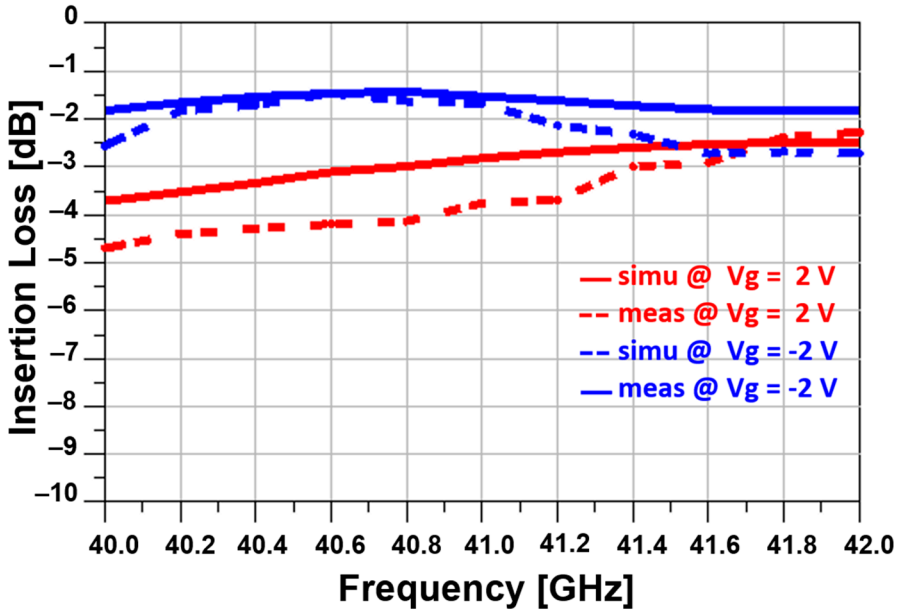

Figure 8. Simulated (continuous line) and measured (dotted line) |S21| versus frequency.

4. Design of Phased Antenna Array

Once the principles of the phase shifter is validated by simulations as well as by measurements. A continuous beam-steerable antenna array operating at 40 GHz is designed and fabricated by inserting this phase shifter into the feeding network. The antenna array is composed of two elements fed by the phase shifter and the dimension after optimization of one element is about 3.4 × 2.4 mm^2, with optimized spacing between elements of 0.47 mm. Figure 9 shows the fabricated prototype of the proposed phased array antenna. This antenna array is also fabricated on a Rogers RT5880 substrate, and the size of the board is about 20 × 16 mm^2.

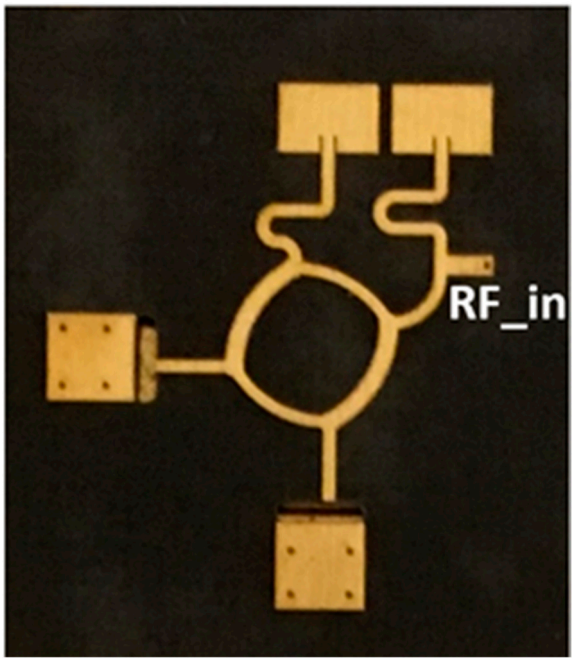

Figure 9. Photograph of fabricated phased antenna array.

Experiments are being carried out to measure the performances of the fabricated phased array and are compared to the simulation results, as can be seen from

Figures 10 and 11. Figure 10 illustrates the simulated and measured reflection coefficients of the phased array antenna. A good agreement between them can be clearly observed and good impedance matching is achieved over the band of 40.50–41.70 GHz.

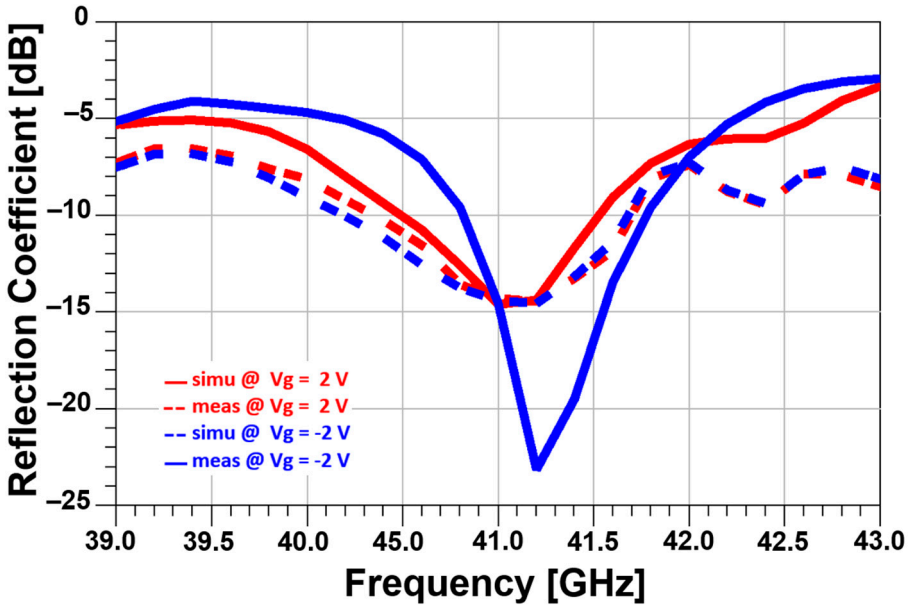

Figure 10. Simulated and measured reflection coefficient for V_g of 2 V and −2 V.

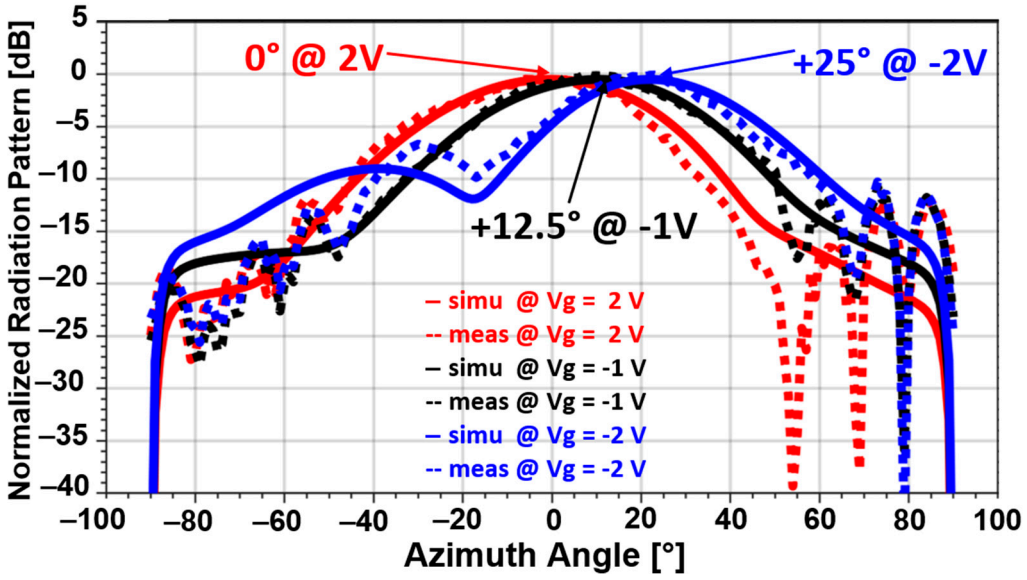

Figure 11. Normalized simulated (continuous line) and measured (dotted line) beam pattern in azimuth at 41 GHz for V_g of 2 V, −1 V, and −2 V.

The total scan patterns of the phased antenna array at the two extreme voltages −2 V and 2 V and at −1 V are shown in Figure 11. By changing the DC bias, beam steering can be achieved since the change in this DC bias has a direct effect on the change in the phase difference between the two radiation elements. Furthermore, the main beam can be tuned continuously to different directions between 0° to 25° by adjusting the phase differences of each antenna element through the phase shifter. A side-lobe level on the azimuth plane around −8 dB is observed for a V_g of −2 V in the measurement, which is a little bit higher compared to the simulated one, which is about −9 dB. This side lobe has occurred at −2 V, which is an extreme DC bias, to achieve the C_{Eqmax} corresponding to a beam scanned at

25° (at C_{Eqmax}). This means that as the scanning angle becomes further from 0° (at C_{Eqmin}), the side lobe appears to become higher. In addition, this can be due to the diffraction of the limited size of the ground conductor and also may be due to some perturbation caused by the PADs used to connect the two varactors using the wire bonding technique.

Thanks to the already developed GaN HEMT varactor small-signal model, the proposed phased antenna array successfully works as was expected in the EM simulations.

5. Conclusions

In this paper, a 41 GHz phased array using GaN HEMT devices for mm wave applications has been presented. This array consists of two antenna patch elements along with a classical phase shifter where two GaN HEMTs are used as varactor diodes to achieve beam steering. The beam of the system can be continuously steered to different directions on the azimuth plane from 0° to 25° by changing the bias voltage of the varactors from −2 to 2 V. Theoretically, this scan range can be easily increased as much as wanted by multiplying the number of the used GaN varactors by a multiple of 2. The compact size, design simplicity, and benefits of GaN technology make this design amenable for implementation in phased array systems, proving to be a suitable candidate for 5G mm-wave communication and beam steering applications.

Author Contributions: GaN device design and measurements, F.M. and M.Z.; GaN data analysis and device modeling, A.H.; conceptualization, A.H., M.H. and O.L.; methodology, A.H., M.H. and O.L.; validation, A.H., M.H. and O.L.; formal analysis, A.H. and M.H.; resources, A.H., M.H., O.L., F.M. and M.Z.; writing—original draft preparation, A.H.; writing—review and editing, A.H. and M.H. All authors have read and agreed to the published version of the manuscript.

Funding: This research received no external funding.

Data Availability Statement: The data are contained within the article.

Conflicts of Interest: The authors declare no conflicts of interest.

References

1. Nallandhigaln, S.N.; Burasa, P.; Wu, K. Deep Integration and Topological Cohabitation of Active Circuits and Antennas for Power Amplification and Radiation in Standard CMOS. *IEEE Trans. Microw. Theory Tech.* **2020**, *68*, 4405–4423. [CrossRef]
2. Chang, K.; York, R.A.; Hall, P.S.; Itoh, T. Active integrated antennas. *IEEE Trans. Microw. Theory Tech.* **2002**, *50*, 937–944. [CrossRef]
3. Hong, W.; Yu, C.; Chen, J.X.; Hao, Z.C. Millimeter wave and terahertz technology. *Sci. China* **2016**, *46*, 1086–1107.
4. Zhang, J.-P.; Zhou, Z.-P. Integrated Architecture of Active Phased Array Antennas for Millimeter Wave Applications. In Proceedings of the 2019 International Symposium on Antennas and Propagation (ISAP), Xi'an, China, 27–30 October 2019; pp. 1–3.
5. Sasikumar, S.; Narayanan, B.S. Analysis of reflective type phase shifter for millimeter wave application. In Proceedings of the 2011 International Conference on Signal Processing, Communication, Computing and Networking Technologies, Thuckalay, India, 21–22 July 2011; pp. 342–346. [CrossRef]
6. Bansal, A.; Panagamuwa, C.J.; Whittow, W.G. State-of-the-Art Millimeter-Wave Beam Steering Antennas for Beyond 5G and 6G Networks: A comprehensive review. *IEEE Antennas Propag. Mag.* **2024**, *66*, 40–51. [CrossRef]
7. Karjalainen, J.; Nekovee, M.; Benn, H.; Kim, W.; Park, J.; Sungsoo, H. Challenges and opportunities of mm-wave communi-cation in 5G networks. In Proceedings of the 2014 9th International Conference on Cognitive Radio Oriented Wireless Networks and Communica-tions (CROWNCOM), Oulu, Finland, 2–4 June 2014; pp. 372–376. [CrossRef]
8. Parker, D.; Zimmermann, D.C. Phased arrays—part 1: Theory and architectures. *IEEE Trans. Microw. Theory Tech.* **2002**, *50*, 678–687. [CrossRef]
9. Khaleel, S.A.; Hamad, E.K.I.; Parchin, N.O.; Saleh, M.B. Programmable Beam-Steering Capabilities Based on Graphene Plasmonic THz MIMO Antenna via Reconfigurable Intelligent Surfaces (RIS) for IoT Applications. *Electronics* **2023**, *12*, 164. [CrossRef]
10. Garver, R.V. Broad-Band Diode Phase Shifters. *IEEE Trans. Microw. Theory Tech.* **1972**, *20*, 314–323. [CrossRef]
11. Kunakovskaya, E.; Ulusoy, A.Ç. An Active Reflection Phase Shifter with High Gain for Reconfigurable Reflectarrays above 0.24 THz. In Proceedings of the IEEE 23rd Topical Meeting on Silicon Monolithic Integrated Circuits in RF Systems, Las Vegas, NV, USA, 22–25 January 2023; pp. 41–43.
12. Chang, C.-H.; Chen, J.-Y.; Shen, C.T.; Tsai, M.-J.; Tai, T.S. Reflection-Type Phase Shifter Integrated with Tunable Power Attenuation Mechanism for Sub-6 GHz Wireless Applications. *IEEE Access* **2022**, *10*, 115532–115540. [CrossRef]

13. Kanoun, M.; Singh Jadav, B.P.; Cordeau, D.; Paillot, J.M.; Mnif, H.; Loulou, M. A Fully Integrated 5.8 GHz BiCMOS SiGe:C tunable active phase shifter for Beamforming. In Proceedings of the 2018 30th International Conference on Microelectronics (ICM), Sousse, Tunisia, 16–19 December 2018; pp. 220–223. [CrossRef]
14. Blosser, C.G.; Sigmarsson, H.H.; Ruyle, J.E. Power Handling of Varactor Diode-Based Frequency Agile Antennas. In Proceedings of the 2022 IEEE International Symposium on Antennas and Propagation and USNC-URSI Radio Science Meeting (AP-S/URSI), Denver, CO, USA, 10–15 July 2022; pp. 1486–1487. [CrossRef]
15. Hamdoun, A.; Roy, L.; Himdi, M.; Lafond, O. Characterisation and analytical modelling of GaN HEMT-based varactor diodes. *IET J. Electron. Lett.* **2015**, *51*, 1930–1932. [CrossRef]
16. Kim, S.; Jang, S.; Lee, J.; Jeong, H.; Kim, K.-J.; Park, C. Ka-Band GaN HEMT Phase Shifter with T-Type Structure for Beamforming Applications. *IEEE Microw. Wirel. Technol. Lett.* **2023**, *33*, 743–746. [CrossRef]
17. Inoue, A. Millimeter-Wave GaN Devices for 5G: Massive MIMO Antenna Arrays for Sub-6-Ghz and mm-Wave Bandwidth. *IEEE Microw. Mag.* **2021**, *22*, 100–110. [CrossRef]
18. Harrouche, K.; Kabouche, R.; Okada, E.; Medjdoub, F. High Performance and Highly Robust AlN/GaN HEMTs for Millimeter-Wave Operation. *IEEE J. Electron Devices Soc.* **2019**, *7*, 1145–1150. [CrossRef]
19. Dogmus, E.; Kabouche, R.; Lepilliet, S.; Linge, A.; Zegaoui, M.; Ben-Ammar, H.; Chauvat, M.-P.; Ruterana, P.; Gamarra, P.; Lacam, C.; et al. InAlGaN/GaN HEMTs at Cryogenic Temperatures. *Electronics* **2016**, *5*, 31. [CrossRef]
20. Hamdoun, A.; Himdi, M.; Roy, L.; Lafond, O. Large Signal and Analytic non-Linear Modelling of GaN HEMT-Based Varactors. In Proceedings of the 2019 IEEE International Conference on Electron Devices and Solid-State Circuits (EDSSC), Xi'an, China, 12–14 June 2019; pp. 1–3. [CrossRef]
21. Garver, R.V. 360° Varactor Linear Phase Modulator. *IEEE Trans. Microw. Theory Tech.* **1969**, *17*, 137–147. [CrossRef]
22. Lucyszyn, S.; Robertson, I.D. Analog reflection topology building blocks for adaptive microwave signal processing applications. *IEEE Trans. Microw. Theory Tech.* **1995**, *43*, 601–611. [CrossRef]
23. RT/duroid® 5870–5880 High Frequency Laminates Data Sheet. Available online: https://www.rogerscorp.com/advanced-electronics-solutions/rt-duroid-laminates/rt-duroid-5880-laminates (accessed on 17 November 2024).
24. Advanced Design System (ADS). Available online: https://www.keysight.com/us/en/products/software/pathwave-design-software/pathwave-advanced-design-system.html (accessed on 17 November 2024).